Nano Research 2013, 6(1): 47–54
DOI 10.1007/s12274-012-0280-8
Research Article

ISSN 1998-0124
CN 11-5974/O4

Mesoporous Co_3O_4 as an electrocatalyst for water oxidation

Harun Tüysüz[1,†], Yun Jeong Hwang[1,‡], Sher Bahadar Khan[2], Abdullah Mohamed Asiri[2], and Peidong Yang[1,2] (✉)

[1] *Department of Chemistry, University of California, Berkeley, California 94720, USA*
[2] *The Center of Excellence for Advanced Materials Research (CEAMR), Chemistry Department, King Abdulaziz University, Jeddah 21589, Saudi Arabia*
[†] *Present address: Max-Planck Institut für Kohlenforschung, Kaiser-Wilhelm-Platz 1, D-45470 Mülheim an der Ruhr, Germany*
[‡] *Present address: Clean Energy Research Center, Korea Institute of Science and Technology, 39-1 Hawolgok-dong, Seongbuk-gu, Seoul 136-791, Republic of Korea*

Received: 3 October 2012
Revised: 13 November 2012
Accepted: 24 November 2012

KEYWORDS
water oxidation,
electrocatalyst,
ordered mesoporous materials,
nanocasting

ABSTRACT

Mesoporous Co_3O_4 has been prepared using porous silica as a hard template via a nanocasting route and its electrocatalytic properties were investigated as an oxygen evolution catalyst for the electrolysis of water. The ordered mesostructured Co_3O_4 shows dramatically increased catalytic activity compared to that of bulk Co_3O_4. Enhanced catalytic activity was achieved with high porosity and surface area, and the water oxidation overpotential (η) of the ordered mesoporous Co_3O_4 decreases significantly as the surface area increases. The mesoporous Co_3O_4 also shows excellent structural stability in alkaline media. After 100 min under 0.8 V (versus Ag/AgCl) applied bias, the sample maintains the ordered mesoporous structure with little deactivation of the catalytic properties.

1 Introduction

Since their discovery in the early 1990s [1, 2], ordered mesoporous materials have become one of the most investigated classes of materials for catalysis [3–5] and other applications, such as sorption [6], separation [7, 8], drug delivery [9, 10], sensors [11, 12], photonics [13], plasmonic [14], fuel cells [15, 16] and magnetism [17, 18]. Recently, ordered mesoporous materials have also attracted considerable attention in the field of direct solar energy conversion to hydrogen production by utilizing various semiconductor compositions such as Ta_2O_5 [19, 20], Ta_3N_4 [21], Nb_2O_5 [22], $BiVO_4$ [23], TiO_2 [24], Al_2O_3/TiO_2 [25], and C_3N_4 [26, 27].

In addition, ordered mesoporous silica based materials, such as MCM-41, SBA-15, and KIT-6, have been used as a support for the deposition of nano-structured materials like CdS [28], $Cd_{1-x}Zn_xS$ [29], Mn_xO_y [30], Co_3O_4 [31] and anchoring of oxo-bridged heterobinuclear units like TiOMn [32] and TiOFe [33]

Address correspondence to p_yang@uclink.berkeley.edu

for photo- and electrocatalytic hydrogen production.

Currently, world energy consumption is based mainly on non-renewable fossil fuels and needs to be shifted to renewable energy sources because of eventual fossil energy supply depletion and climate change concerns due to carbon dioxide accumulation in the atmosphere. The renewable hydrogen produced by photo- and electrochemical splitting of water is one of the most promising alternative clean energy sources. Water splitting can be catalyzed by several inorganic semiconductors, the first of which, TiO_2, was discovered in the early 1970s by Fujishima and Honda [34]. Following this report, numerous electrochemical and photochemical water splitting studies on various metal oxides as catalytic materials for hydrogen and oxygen evolution have been conducted [35–46].

Metal or metal oxide co-catalysts are often employed to facilitate solar water splitting reactions. The main function of the co-catalysts is to lower the electrochemical overpotentials related to the multi-electron water oxidation and reduction reactions. For the water oxidation half reaction, noble metal oxides such as ruthenium oxide and iridium oxide are the most active oxidation catalysts [47]. However, these elements are expensive and less abundant, thus making them unsuitable to use on a large scale. Therefore, it is important to develop catalysts composed of more abundant elements. Nowadays, there is great interest in the development of novel co-catalyst materials that do not consist of precious metals. The recent study of Nocera et al. where amorphous Co-oxyphosphates were used as water oxidation catalysts was found to be quite promising [48]. Some transition metal oxides such as oxides of Fe, Mn, Ni, and Co [49, 50] have also been investigated. Recently Esswein et al. reported the size-dependent activity of Co_3O_4 nanoparticle anodes for alkaline water electrolysis [51]. They observed a maximal activity for nanoparticles having the highest surface area. Their electrochemical study indicates the promise of Co_3O_4 materials for the development of efficiently nanostructured catalysts for water oxidation with comparable overpotential to that of RuO_2.

In this study, we report on the electrocatalytic activity of ordered mesoporous Co_3O_4 for water electrolysis with enhanced catalytic activity because of its large porosity and high surface area. By taking advantage of the well-established nanocasting method, a series of highly ordered crystalline mesoporous Co_3O_4 materials with various particle size, porosity and surface area were prepared, and the catalytic activities of these materials were investigated for electrochemical water splitting.

2 Experimental

2.1 Material preparation

Cubic ordered mesoporous KIT-6 was prepared according to the Ref. [52]. Briefly, 13.5 g of surfactant (Pluronic 123, $EO_{20}PO_{70}EO_{20}$) was dissolved in a mixture of 487.5 g of distilled water and 26.1 g of concentrated HCl (37%). 13.5 g *n*-butanol was added to the homogenous solution at 35 ℃. After stirring the solution for 1 h, 29 g of tetraethyl orthosilicate (TEOS) was quickly added to the solution and followed by stirring at the same temperature for 24 h. The mixture was then heated at different temperatures (35, 100 or 130 ℃) for another 24 h under static conditions (for an aging temperature of 130 ℃, the mixture was transferred into an autoclave). The solid product was filtered without washing, dried at 90 ℃ overnight, and then calcined at 550 ℃ for 6 h.

KIT-6, with different textural parameters, was used as the hard template to fabricate cubic ordered mesoporous Co_3O_4. In a typical synthesis, 0.5 g of KIT-6 was dispersed in 5 mL of 0.8 M $Co(NO_3)_2{\cdot}6H_2O$ in ethanol and stirred for 1 h at room temperature. Subsequently, the ethanol was evaporated at 50 ℃. The sample was calcined at 200 ℃ for 6 h. The composite was re-impregnated again, followed by calcination at 450 ℃ for 6 h (with an intermediate plateau at 200 ℃ for 4 h). The silica template was then removed using 2 M NaOH aqueous solution.

2.2 Working electrode preparation and electrochemical measurements

A gold electrode (5 mm diameter, Pine Research Instrumentation AFE1E050AU) loaded with Co_3O_4 was chosen as a working electrode. The surface of the gold disk electrode (GE) was polished with sandpaper and diamond suspension with different particle sizes (6, 1, and 0.25 μm) to obtain a clean surface. After

polishing, 5 μL of a 0.02 M ethanol solution of Co_3O_4 (0.13 mg/cm²), which was sonicated for at least 30 min, was dropped on a GE and dried at room temperature. Subsequently, 5 μL of a 0.25 wt.% Nafion solution was dropped on the GE as the binding agent. Finally, the electrode was dried in a vacuum oven at 120 °C for 2 h. Catalytic current measurements were performed in aqueous KOH electrolytes with a three electrode configuration (EG&G Princeton Applied Research Potentiostat, VersaSTAT Ⅱ), consisting of a GE loaded with Co_3O_4 as the working electrode, a Pt gauze as the counter electrode, and a Ag/AgCl reference electrode. All three electrodes were fixed in a glass cell to retain the distance between electrodes, and Ar gas was bubbled through to remove the dissolved oxygen during the measurements. All the current versus potential measurements were carried out at a 50 mV/s sweep rate. Chronoamperometric measurements were carried out in 0.1 M KOH solution by applying a bias of 0.8 V (vs. Ag/AgCl) for 10 min and zero current for an additional 10 min sequentially.

3 Results and discussion

The morphology, structure, porosity and textural parameters of nanocast Co_3O_4 can be controlled by using an appropriate silica hard template. In this study, we prepared three different ordered mesoporous Co_3O_4 structures. A detailed structure analysis of the Co_3O_4 replica has been discussed elsewhere [53]. Transmission electron microscopy (TEM) images of the nanocast Co_3O_4 samples are presented in Fig. 1.

The ordered structure of all samples can be clearly seen from the images. Co_3O_4-35 (35 indicates the aging temperature of the silica hard template), which was fabricated from KIT-6 aged at low temperature, has a more open uncoupled sub-framework structure while Co_3O_4-100, and Co_3O_4-130 have a dense coupled framework as expected due to the different interconnectivity between the channels of the KIT-6 hard template [53]. TEM indicated that the domain sizes of the samples are in the range of several hundred nm and the crystallite size of the Co_3O_4-35, Co_3O_4-100, and Co_3O_4-130 are around 6, 8, and 10 nm, respectively. The surface areas (SA) of the samples were determined by using the N_2-sorption technique. As shown in Table 1, Co_3O_4-35 had a surface area of 156 m²/g, while those of Co_3O_4-100 and Co_3O_4-130 were 113 and 72 m²/g, respectively. By increasing the aging temperature of the silica hard template, the surface area of the nanocast

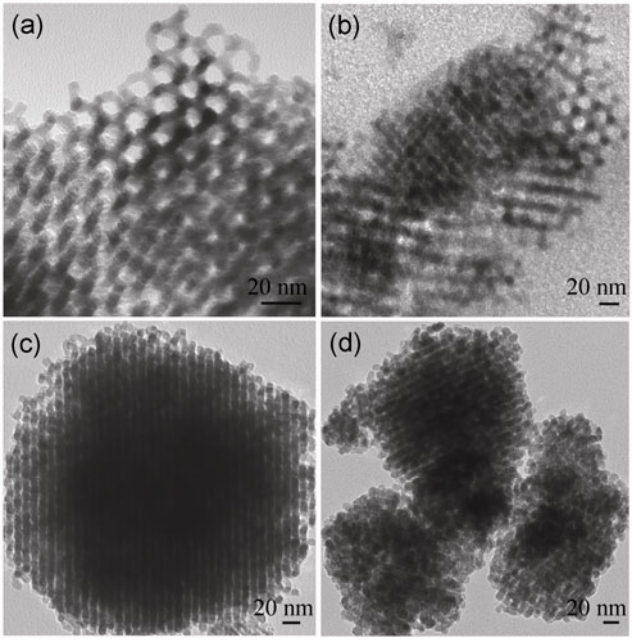

Figure 1 TEM images of Co_3O_4-35 (a), Co_3O_4-100 (c), Co_3O_4-130 (d), and Co_3O_4-35 after electrochemical measurement (b).

Table 1 Overpotential (at 5 and 10 mA/cm²) and current density (at 1 V vs. Ag/AgCl) of commercial (bulk) and various cubic ordered mesoporous Co_3O_4 materials at pH 13 (0.1 M KOH)

	BET SA (m^2/g)	Crystallite size (nm)	Overpotential (mV) at 5 mA/cm²	Overpotential (mV) at 10 mA/cm²	Current density (mA/cm²) at overpotential 735 mV
GE	—	—	—	—	1.6
Co_3O_4 Bulk	2	μm range	—	—	2.8
Co_3O_4-130	72	10	592	—	8.7
Co_3O_4-100	113	8	486	636	13.6
Co_3O_4-35	156	6	453	525	27.2

Co_3O_4 decreases because of the increasing pore size of the silica template, generating a replica with a larger crystallite size.

Co_3O_4 is an active electrocatalyst for oxygen evolution in alkaline conditions. We have investigated electrocatalytic properties of nanocast Co_3O_4 series in water splitting. The linear sweeps of a bare gold electrode, commercial Co_3O_4, and ordered mesoporous Co_3O_4-35, Co_3O_4-100, and Co_3O_4-130 loaded gold electrodes in 0.1 M KOH solution (pH 13) are given in Fig. 2.

Here, the potential for the anode $E^{\circ}_{OH^-/O_2}$ = 0.463 V vs. the normal hydrogen electrode (NHE) at pH 13—which corresponds to 0.265 V vs. the Ag/AgCl reference electrode—was used for all overpotential measurements. The overpotentials of bulk and nanocast Co_3O_4 samples at a specified current density (5 mA/cm^2 or 10 mA/cm^2) and the current densities observed at 1 V (vs. Ag/AgCl) are presented in Table 1. The commercial Co_3O_4 shows the lowest current density while Co_3O_4-35 reveals the highest current density at a given potential. Commercial Co_3O_4 reaches a current density of 2.8 mA/cm^2 while with ordered mesoporous Co_3O_4-130, Co_3O_4-100, and Co_3O_4-35, current densities of 8.7, 13.6, and 27.2 mA/cm^2 can be achieved at 1 V (vs. Ag/AgCl, or an overpotential of 735 mV). A current density of 5 mA/cm^2 was obtained at 857, 751, and 718 mV (vs. Ag/AgCl) for Co_3O_4-130, Co_3O_4-100, and Co_3O_4-35, respectively, corresponding to overpotentials of 592, 486, and 453 mV, respectively.

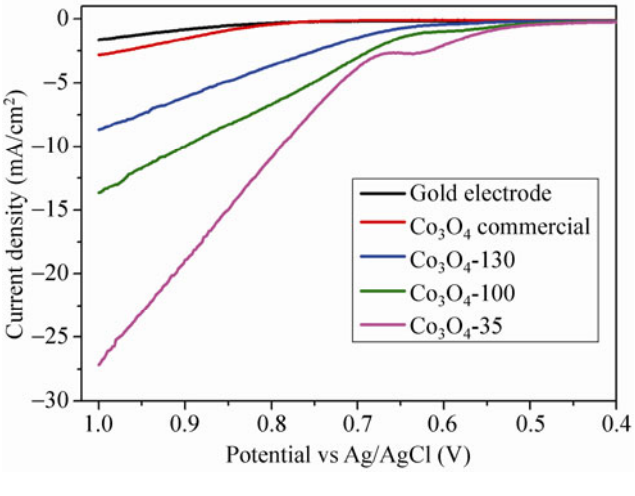

Figure 2 Linear voltammograms of a bare gold electrode, and commercial bulk and nanocast Co_3O_4 samples.

To compare electrocatalytic activity of the mesoporous structure with that of nanoparticles, we also prepared Co_3O_4 nanoparticles through hydrothermal synthesis according to the Ref. [54]. TEM investigation indicated that (Fig. S1(a) in the Electronic Supplementary Material (ESM)) the nanoparticles were not very uniform in size with an average particle size of 5 nm. Linear voltammograms of Co_3O_4 with ordered mesoporous structure and nanoparticle morphologies in 0.1 M KOH solution are shown in Fig. S1(b) (in the ESM). It can be seen that the two types of nanostructures exhibit comparable activities. One key advantage of using ordered mesoporous structures over nanoparticles is the easy dispersion and formation of a stable film on working electrode. Although nanocasting is more time consuming in comparison with hydrothermal synthesis, the flexible synthetic process allows the synthesis of composite nanostructures with precisely controlled composition, crystallite size, and interconnectivity for electrochemical applications.

Assuming that the Faraday efficiency is 100% and that every Co atom is an active site (lower bound of activity), the turnover frequency (TOF) for oxygen evolution can be calculated from the anodic current density. At 400 mV of overpotential, commercial Co_3O_4 particles exhibit a TOF of 0.142×10^{-3} s^{-1} on a GE electrode, while the ordered mesoporous Co_3O_4-130, Co_3O_4-100, and Co_3O_4-35 achieve TOFs of 1.58×10^{-3} s^{-1}, 3.16×10^{-3} s^{-1}, and 4.55×10^{-3} s^{-1}, respectively, under the same conditions. The TOFs of mesoporous Co_3O_4-130, Co_3O_4-100, and Co_3O_4-35 are respectively 11, 22, and 32 times larger than that of commercial Co_3O_4. Comparison of the TOFs and overpotentials of various Co_3O_4 anodes prepared in this study illustrates the importance of a large surface for high catalytic activity.

Electrolyte type and the concentration used are important parameters for electrochemical reactions. Typically, a concentrated alkali solution is used as the electrolyte for oxygen evolution in the cases of basic metal oxides like Co_3O_4. A series of KOH solutions with different pH was prepared to investigate the effect of different concentrations of alkali solutions on the electrocatalytic activity of the nanocast Co_3O_4-35. Plots of current density vs. potential for various pH solutions are presented in Fig. 3. Relatively low

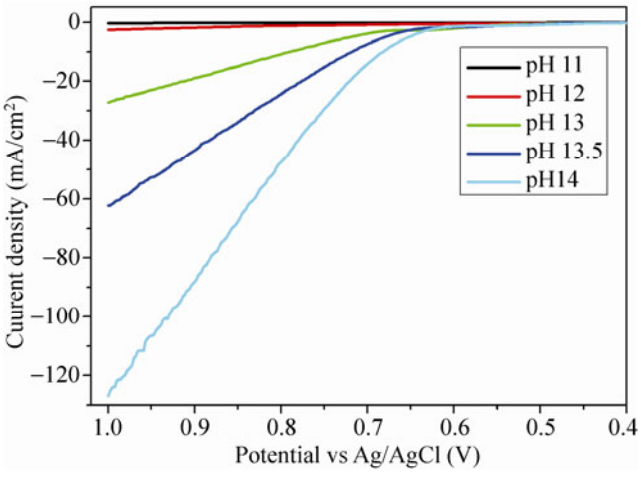

Figure 3 Linear voltammograms of Co_3O_4-35 in solutions with various KOH concentrations.

current densities were observed at pH 11 and 12, (0.3 and 2.6 mA/cm² at 1 V vs. Ag/AgCl). However, the effect of the alkali solution concentration becomes more apparent at pH 13, where a current density of 27.2 mA/cm² at 1 V (vs. Ag/AgCl) was obtained. Further increasing the solution pH to 13.5 or 14 gives a higher current density of 62.3 and 126.9 mA/cm² at 1 V (vs. Ag/AgCl), respectively. To compare the catalytic activities at different pH, the thermodynamic potentials (and hence catalyst overpotentials) were calculated at particular current densities. As seen from Table 2, overpotentials of 646, 541, and 514 mV were measured at 20 mA/cm² current density for pH 13, 13.5, and 14, respectively. These results suggest that the oxidative catalytic activity of the mesoporous Co_3O_4 increases with increasing concentration of OH^- ions in the electrolyte.

Besides catalytic activity, material stability is also a critical issue in order to develop cost effective catalysts for water splitting. Although RuO_2 is the most active material for oxygen evolution, it is generally unstable at high overpotential. RuO_2 easily dissolves as ruthenate in basic solutions or dissolves as volatile RuO_4 if the potentials for the oxidation of surface sites to Ru(Ⅵ) or Ru(Ⅷ) are reached [47]. Co_3O_4 has gained more attention due to its strong stability and realistic affordability.

Figure 4 shows a chronoamperometric measurement of the Co_3O_4-35 sample biased at 0.8 V vs. Ag/AgCl at pH 13 for 100 min. At that potential, the sample reaches

Table 2 Overpotential (at 10 and 20 mA/cm²) and current density (at 1 V vs. Ag/AgCl) of cubic ordered mesoporous Co_3O_4-35 at different pH

	Overpotential (mV) at 10 mA/cm²	Overpotential (mV) at 20 mA/cm²	Current density (mA/cm²) at 1 V (vs. Ag/AgCl)
pH 11	—	—	0.3
pH 12	—	—	2.6
pH 13	525	646	27.2
pH 13.5	483	541	62.3
pH 14	476	514	126.9

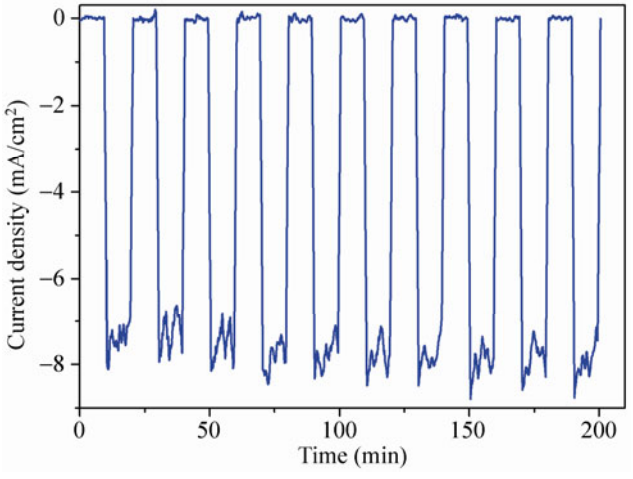

Figure 4 Chronoamperometric measurement of the Co_3O_4-35 sample biased at 0.8 V vs. Ag/AgCl at pH 13 for 100 min.

a current density of 8 mA/cm² and does not show any deactivation over 100 min, despite the high surface area and nanocrystalline structure.

The TEM image of this sample after 100 min under bias still shows the presence of an ordered mesoporous structure with 6 nm average crystallite size (Fig. 1(b)). This finding provides solid evidence for the structural stability of nanocast Co_3O_4-35, making it a promising electrocatalyst for oxygen evolution.

4 Conclusion

We have presented the design of a series of ordered mesoporous Co_3O_4 materials by using the nanocasting route and the catalytic activities of these materials were investigated in electrochemical water splitting. It was found that the electrocatalytic activities of the samples significantly depend on the structure, surface

area, and pH of electrolyte solution. The highest catalytic activity was achieved in a more concentrated alkali solution with Co_3O_4 that has an open sub-framework structure and high surface area. As the surface area increases, the overpotential decreases significantly. Cubic ordered mesoporous Co_3O_4 has excellent structural stability during the electrolysis of water; this material holds promise as a cheap anode for overall water splitting. A further study combining the use of this nanocast Co_3O_4 with high surface area semiconductor materials for photo–electrochemical water splitting is in progress.

Acknowledgements

This work was funded by King Abdulaziz University (KAU), under grant No. (HiCi/30-3-1432). The authors, therefore, acknowledge technical and financial support of KAU. H. Tüysüz thanks the German Research Foundation (DFG) for his research fellowship.

Electronic Supplementary Material: Supplementary material (TEM image of Co_3O_4 nanoparticles and linear voltammograms of Co_3O_4 with ordered mesoporous and nanoparticle morphologies) is available in the online version of this article at http://dx.doi.org/10.1007/s12274-012-0280-8.

References

[1] Yanagisawa, T.; Shimizu, T.; Kuroda, K.; Kato, C. The preparation of alkyltrimethylammonium-kanemite complexes and their conversion to microporous materials. *Bull. Chem. Soc. Jpn.* **1990**, *63*, 988–992.

[2] Kresge, C. T.; Leonowicz, M. E.; Roth, W. J.; Vartuli, J. C.; Beck, J. S. Ordered mesoporous molecular sieves synthesized by a liquid-crystal template mechanism. *Nature* **1992**, *359*, 710–712.

[3] Corma, A. From microporous to mesoporous molecular sieve materials and their use in catalysis. *Chem. Rev.* **1997**, *97*, 2373–2419.

[4] Tüysüz, H.; Comotti, M.; Schüth, F. Ordered mesoporous Co_3O_4 as highly active catalyst for low temperature CO-oxidation. *Chem. Commun*. **2008**, 4022–4024.

[5] Taguchi, A.; Schüth, F. Ordered mesoporous materials in catalysis. *Micropor. Mesopor. Mater.* **2005**, *77*, 1–45.

[6] Kruk, M.; Jaroniec, M. Gas adsorption characterization of ordered organic–inorganic nanocomposite materials. *Chem. Mater.* **2001**, *13*, 3169–3183.

[7] MacLachlan, M. J.; Coombs, N.; Ozin, G. A. Non-aqueous supramolecular assembly of mesostructured metal germanium sulphides from $(Ge_4S_{10})^{4-}$ clusters. *Nature* **1999**, *397*, 681–684.

[8] Martin, T.; Galarneau, A.; Di Renzo, F.; Brunel, D.; Fajula, F.; Heinisch, S.; Cretier, G.; Rocca, J. L. Great improvement of chromatographic performance using MCM-41 spheres as stationary phase in HPLC. *Chem. Mater.* **2004**, *15*, 1725–1731.

[9] Mellaerts, R.; Aerts, C. A.; Van Humbeeck, J.; Augustijns, P.; Van den Mooter, G.; Martens, J. A. Enhanced release of itraconazole from ordered mesoporous SBA-15 silica materials. *Chem. Commun*. **2007**, 1375–1377.

[10] Yang, P. P.; Quan, Z. W.; Lu, L. L.; Huang, S. S.; Lin, J.; Fu, H. G. MCM-41 functionalized with YVO_4:Eu^{3+}: A novel drug delivery system. *Nanotechnology* **2007**, *18*, 235703.

[11] Hyodo, T.; Nishida, N.; Shimizu, Y.; Egashira, M. Preparation and gas-sensing properties of thermally stable mesoporous SnO_2. *Sensors and Actuators B* **2002**, *83*, 209–215.

[12] Shenderovich, I. G.; Buntkowsky, G.; Schreiber, A.; Gedat, E.; Sharif, S.; Albrecht, J.; Golubev, N. S.; Findenegg, G. H.; Limbach, H. H. Pyridine-^{15}N – A mobile NMR sensor for surface acidity and surface defects of mesoporous silica. *J. Phys.Chem. B* **2003**, *107*, 11924–11939.

[13] Fuertes, M. C.; López-Alcaraz, F. J.; Marchi, M. C.; Troiani, H. E.; Luca, V.; Míguez, H.; Soler-Illia, G. J. A. A. Photonic crystals from ordered mesoporous thin-film functional building blocks. *Adv. Funct. Mater.* **2007**, *17*, 1247–1254.

[14] Aznar, E.; Marcos, M. D.; Martínez-Máñez, R.; Sancenón, F.; Soto, J.; Amorós, P.; Guillem, C. pH- and photo-switched release of guest molecules from mesoporous silica supports. *J. Am. Chem. Soc.* **2009**, *131*, 6833–6843.

[15] Ding, J.; Chan, K, Y.; Ren, J.; Xiao, F. S. Platinum and platinum–ruthenium nanoparticles supported on ordered mesoporous carbon and their electrocatalytic performance for fuel cell reactions. *Electrochem. Acta* **2005**, *50*, 3131–3141.

[16] Ji, X.; Lee, K. T.; Nazar, L. F. A highly ordered nanostructured carbon–sulphur cathode for lithium–sulphur batteries. *Nat. Mater.* **2009**, *8*, 500–506.

[17] Lu, A. H.; Schmidt, W.; Matoussevitch, N.; Bönnermann, H.; Spliethoff, B.; Tesche, B.; Bill, E.; Kiefer, W.; Schüth, F. Nanoengineering of a magnetically separable hydrogenation catalyst. *Angew. Chem. Int. Ed*. **2004**, *43*, 4303–4306.

[18] Tüysüz, H.; Salabas, E. L.; Weidenthaler, C.; Schüth, F. Synthesis and magnetic investigation of ordered mesoporous two-line ferrihydrite. *J. Am. Chem. Soc.* **2008**, *130*, 280–287.

[19] Takahara, Y.; Kondo, J. N.; Takata, T.; Lu, D.; Domen, K. Mesoporous tantalum oxide. 1. Characterization and photocatalytic activity for the overall water decomposition. *Chem. Mater.* **2001**, *13,* 1194–1199.

[20] Noda, Y.; Lee, B.; Domen, K.; Kondo, J. N. Synthesis of crystallized mesoporous tantalum oxide and its photocatalytic activity for overall water splitting under ultraviolet light irradiation. *Chem. Mater.* **2008**, *20,* 5361–5367.

[21] Hisatomi, T.; Otani, M.; Nakajima, K.; Teramura, K.; Kako, Y.; Lu, D.; Takata, T.; Kondo, J. N.; Domen, K. Preparation of crystallized mesoporous Ta_3N_5 assisted by chemical vapor deposition of tetramethyl orthosilicate. *Chem. Mater.* **2010**, *22*, 3854–3861.

[22] Chen, X.; Yu, T.; Fan, X.; Zhang, H.; Li, Z.; Ye, J.; Zou, Z. Enhanced activity of mesoporous Nb_2O_5 for photocatalytic hydrogen production. *Appl. Surf. Sci.* **2007**, *253*, 8500–8506.

[23] Li, G.; Zhang, D.; Yu. J. C. Ordered mesoporous $BiVO_4$ through nanocasting: A superior visible light-driven photocatalyst. *Chem. Mater.* **2008**, *20,* 3983–3992.

[24] Zhang, Z.; Zuo, F.; Feng, P. Hard template synthesis of crystalline mesoporous anatase TiO_2 for photocatalytic hydrogen evolution. *J. Mater. Chem*. **2010**, *20*, 2206–2212.

[25] Kim, J. Y.; Kang, S. H.; Kim, H. S.; Sung, Y. E. Preparation of highly ordered mesoporous Al_2O_3/TiO_2 and its application in dye-sensitized solar cells. *Langmuir* **2010**, *26*, 2864–2870.

[26] Chen, X.; Jun, Y. S.; Takanabe, K.; Maeda, K.; Domen, K.; Fu, X. Z.; Antonietti, M.; Wang, X. C. Ordered mesoporous SBA-15 type graphitic carbon nitride: A semiconductor host structure for photocatalytic hydrogen evolution with visible light. *Chem. Mater.* **2009**, *21*, 4093–4095.

[27] Wang, X. C.; Maeda, K.; Thomas, A.; Takanabe, K.; Xin, G.; Carlsson, J. M.; Domen, K.; Antonietti, M. A metal-free polymeric photocatalyst for hydrogen production from water under visible light. *Nat. Mater.* **2009**, *8*, 76–80.

[28] Ryu, S. Y.; Balcerski, W.; Lee, T. K.; Hoffmann, M. R. Photocatalytic production of hydrogen from water with visible light using hybrid catalysts of CdS attached to microporous and mesoporous silica. *J. Phys. Chem. C* **2007**, *111,* 18195–18203.

[29] Macias-Sanchez, S. A.; Nava, R.; Hernandez-Morales, V.; Acosta-Silva, Y. J.; Gomez-Herrera, L.; Pawelec, B.; Al-Zahrani, S. M.; Navarro, R. M.; Fierro, J. L. G. $Cd_{1-x}Zn_xS$ solid solutions supported on ordered mesoporous silica (SBA-15): Structural features and photocatalytic activity under visible light. *Int. J. Hydrog. Energy* **2012**, *37*, 9948–9958.

[30] Jiao, F.; Frei, H. Nanostructured manganese oxide clusters supported on mesoporous silica as efficient oxygen-evolving catalysts. *Chem. Commun*. **2010**, *46*, 2920–2922.

[31] Jiao, F.; Frei, H. Nanostructured cobalt oxide clusters in mesoporous silica as efficient oxygen-evolving catalysts. *Angew. Chem. Int. Ed.* **2009**, *48*, 1841–1844.

[32] Cuk, T.; Weare, W. W.; Frei, H. Unusually long lifetime of excited charge-transfer state of all-inorganic binuclear $TiOMn^{II}$ unit anchored on silica nanopore surface. *J. Phys. Chem. C* **2010**, *114*, 9167–9172.

[33] Okamoto, A.; Nakamura, R.; Osawa, H.; Hashimoto, K. Site-specific synthesis of oxo-bridged mixed-valence binuclear complexes on mesoporous silica. *Langmuir* **2008**, *24*, 7011–7017.

[34] Fujishima, A.; Honda, K. Electrochemical photolysis of water at a semiconductor electrode. *Nature* **1972**, *238*, 37–38.

[35] Ikeda, S.; Takata, T.; Kondo, T.; Hitoki, G.; Hara, M.; Kondo, J. N.; Domen, K.; Hosono, H.; Kawazoe, H.; Tanaka, A. Mechano-catalytic overall water splitting. *Chem. Commun*. **1998**, 2185–2186.

[36] Takata, T.; Tanaka, A.; Hara, M.; Kondo, J. N.; Domen, K. Recent progress of photocatalysts for overall water splitting. *Catal. Today* **1998**, *44*, 17–26.

[37] Kim, H. G.; Hwang, D. W.; Kim, J.; Kim, Y. G.; Lee, J. S. Highly donor-doped (110) layered perovskite materials as novel photocatalysts for overall water splitting. *Chem. Commun*. **1999**, 1077–1078.

[38] Kudo, A.; Kato, H.; Nakagawa, S. Water splitting into H_2 and O_2 on new $Sr_2M_2O_7$ (*M* = Nb and Ta) photocatalysts with layered perovskite structures: Factors affecting the photocatalytic activity. *J. Phys. Chem. B* **2000,** *104*, 571–575.

[39] Kato, H.; Asakura, K.; Kudo, A. Highly efficient water splitting into H_2 and O_2 over lanthanum-doped $NaTaO_3$ photocatalysts with high crystallinity and surface nanostructure. *J. Am. Chem. Soc.* **2003**, *125*, 3082–3089.

[40] Khan, S. U. M.; Al-Shahry, M.; Ingler, W. B. Efficient photochemical water splitting by a chemically modified n-TiO_2. *Science* **2002**, *297*, 2243–2245.

[41] Maeda, K.; Takata, T.; Hara, M.; Saito, N.; Inoue, Y.; Kobayashi, H.; Domen, K. GaN:ZnO solid solution as a photocatalyst for visible-light-driven overall water splitting. *J. Am. Chem. Soc*. **2005**, *127*, 8286–8287.

[42] Maeda, K.; Teramura, K.; Lu, D.; Takata, T.; Saito, N.; Inoue, Y.; Domen, K. Photocatalyst releasing hydrogen from water. *Nature* **2006**, *440*, 295.

[43] Mor, G. K.; Shankar, K.; Paulose, M.; Varghese, O. K.; Grimes, C. A. Enhanced photocleavage of water using titania nanotube arrays. *Nano Lett.* **2005**, *5*, 191–195.

[44] Cesar, I.; Kay, A.; Martinez, J. A. G.; Grätzel, M. Translucent thin film Fe_2O_3 photoanodes for efficient water splitting by sunlight: Nanostructure-directing effect of Si-doping. *J. Am. Chem. Soc*. **2006**, *128*, 4582–4583.

[45] Sivula, K.; Le Formal, F.; Gräetzel, M. Solar water splitting: Progress using hematite (α-Fe_2O_3) photoelectrodes. *ChemSusChem* **2011**, *4*, 432–449.

[46] Tilley, S. D.; Cornuz, M.; Sivula, K.; Gräetzel, M. Light-induced water splitting with hematite: Improved nanostructure and iridium oxide catalysis. *Angew. Chem. Int. Ed.* **2010**, *49*, 6405–6408.

[47] Walter, M.; Warren, E. L.; Boettcher, S. W.; Mi, Q.; Mckone, J. R.; Santori, E. A.; Lewis, N. S. Solar water splitting cells. *Chem. Rev.* **2010**, *110*, 6446–6473.

[48] Surendranath, Y.; Dincă, M.; Nocera, D. G. Electrolyte-dependent electrosynthesis and activity of cobalt-based water oxidation catalysts. *J. Am. Chem. Soc.* **2009**, *131*, 2615–2620.

[49] Harriman, A.; Pickering, I. J.; Thomas, J. M.; Christensen, P. A. Metal oxides as heterogenous catalysts for oxygen evolution under photochemical conditions. *J. Chem. Soc., Faraday Trans. 1* **1988**, *84*, 2795–2806.

[50] Khan, S. U. M.; Akikusa, J. Stability and photoresponse of nanocrystelline n-TiO_2 and n-TiO_2/Mn_2O_3 thin film electrodes during water splitting reactions. *J. Electrochem. Soc.* **1998**, *145*, 89–93.

[51] Esswein, A.; McMurdo, M. J.; Ross, P. N.; Bell, A. T.; Tilley, T. D. Size-dependent activity of Co_3O_4 nanoparticle anodes for alkaline water electrolysis. *J. Phys. Chem. C* **2009**, *113*, 15068–15072.

[52] Kleitz, F.; Choi, S. H.; Ryoo, R. Cubic *Ia3d* large mesoporous silica: Synthesis and replication to platinum nanowires, carbon nanorods and carbon nanotubes. *Chem. Commun.* **2003**, 2136–2137.

[53] Tüysüz, H.; Lehmann, C. W.; Bongard, H.; Tesche, B.; Schmidt, R.; Schüth, F. Direct imaging of surface topology and pore system of ordered mesoporous silica (MCM-41, SBA-15, and KIT-6) and nanocast metal oxides by high resolution scanning electron microscopy. *J. Am. Chem. Soc.* **2008**, *130*, 11510–11517.

[54] Dong, Y. M.; He, K.; Yin, L.; Zhang, A. M. A facile route to controlled synthesis of Co_3O_4 nanoparticles and their environmental catalytic properties. *Nanotechnology* **2007**, *18*, 435602.